Journal of Applied Fluid Mechanics, Vol. 10, No. 6, pp. 1657-1668, 2017.
Available online at www.jafmonline.net, ISSN 1735-3572, EISSN 1735-3645.
DOI: 10.29252/jafm.73.245.27675

Entropy Production Analysis for S-Characteristics of a Pump Turbine

R. Z. Gong[1†], N. M. Qi[2], H. J. Wang[1†], A. L. Chen[1] and D. Q. Qin[1,3]

[1]*Department of Energy Science and Engineering, Harbin Institute of Technology, Harbin, 150001, China*
[2] *School of Astronautics, Harbin Institute of Technology, Harbin, 150001, China*
[3] *State Key Laboratory of Hydro-Power Equipment, Harbin Institute of Large Electrical Machinery, Harbin, 150046, China*

†*Corresponding Author Email: gongruzhi@hit.edu.cn*

(Received February 10, 2017; accepted August 9, 2017)

ABSTRACT

Due to the S-shape characteristics and the complicated flow in pump turbine, there may be serious instability when the pump-storage power plant starts. In order to conduct further study on the energy dissipation in hydraulic turbine, three dimensional incompressible steady state simulations were applied using SST k-ω turbulence model in this paper. It can be seen that the simulation results are consistent with experimental results well by the comparison of characteristic curves, and further analyses were made based on the entropy production theory. It is shown that the entropy production of spiral casing accounts for the minimum proportion in all components. The entropy production of cascades and runner differs a lot at different guide vane openings, and it features "S" characteristics with the increase of discharge. Then, the analysis of entropy production distribution on runner, blade cascades and draft tube was carried out at the 10mm guide vane opening. It was found that the losses in guide vane space is much higher than that of stay vane space and the losses are mainly in the tail area of stay vanes and vaneless space. The losses mainly occurs in the leading edges and the trailing edges of blades. The largest losses mainly lie at the wall of straight cone near the inlet in draft tube. The losses at the inner surface of elbow are also very high. The results indicate that the method based on the entropy production theory is very helpful to analyze and locate the losses in hydraulic turbine.

Keywords: Hydraulic turbine; S-shape characteristics; Entropy production; Energy losses.

NOMENCLATURE

D_1	runner inlet diameter
g	acceleration due to gravity
H	hydraulic head of turbine
Hg	height of guide vane
k	kinetic energy of the turbulent fluctuations
P_{in}	average pressure at spiral casing inlet
P_{out}	average pressure at draft tube outlet
Q	the discharge
$\dot{Q}$	energy transfer rate
R_1	runner inlet radius
$\dot{S}_D$	whole entropy production rate for turbulent flows
$\dot{S}_{\overline{D}}$	entropy production rate due to the time-averaged movement
$\dot{S}_{D'}$	entropy production rate due to velocity fluctuations
$\dot{S}_D^{'''}$	specific entropy production rate
$\dot{S}_{\overline{D}}^{'''}$	specific entropy production rate due to the time-averaged movement
$\dot{S}_{D'}^{'''}$	specific entropy production rate due to velocity fluctuations
T	torque of the runner
$\overline{u_1}$, $\overline{u_2}$, $\overline{u_3}$	time-averaged velocity components
u_1', u_2', u_3'	velocity fluctuation components
Z_b	number of runner blades
Zg	number of guide vanes
Zs	number of stay vanes
ε	dissipation rate of kinetic energy
η	efficiency of turbine
λ	torque coefficient
μ	viscosity of fluid
μ_{eff}	effective viscosity
μ_t	the turbulent viscosity
ρ	density of fluid
φ	discharge coefficient
ψ	head coefficient

Ω	rotational speed of turbine runner	ω	represents the characteristic frequency

1. INTRODUCTION

Hydropower is a kind of renewable clean energy, which is an important part of world's energy. In this regard, hydropower policies and renewable energy investments recently gain impetus. Pumped storage power plant has the ability of flexible adjustment, so it is of great significance to the safe and stable operation of power network. As the key component of the hydropower station, the pump turbine has many unstable performance. While the design of hydraulic turbine still a key step of hydro-energy industry, because the characteristic curve of pump turbine has a so called S-shape characteristic when the pump turbine is under the operating conditions of first quadrant or fourth quadrant, where the same unit speed may correspond to different discharge, which will result in serious instability of power plant when it starts even not being connected to power grid. Therefore it is very important to do a further research about it. Energy dissipation happens in the internal flow of a hydro-machine, which is irreversible and causes losses which will lead to entropy production. From the view of thermodynamics, energy dissipation converts the available energy to unavailable energy along with entropy production. A great deal of research has been carried out about entropy production. Herwig *et al*. (2008) pointed out that the local dissipation rates in the flow can be determined with entropy production, which was validated with experimental data for laminar and turbulent flows. Zhang *et al*. (2009) conducted entropy production is a direct measure of the losses flow. For many areas, entropy serves as a key parameter in achieving the upper limits of operation performance (Naterer *et al*. 2008). The entropy rate could be obtained based on the computational parameters getting from commercial CFD software. However, pressure drop can be expressed with entropy and temperature, so we could get the detailed flow losses for every position.

Recently, some researchers have applied this theory to calculate energy dissipations of flow. For example, Ghasemi *et al*. (2013) predicted the integral entropy production rate and the skin friction coefficient in the transition region. Recent literatures on the topic of entropy production in wall-bounded flow have been reviewed by Naterer *et al*. (2008) and others(Mceligot *et al*. 2008a, Mceligot *et al*. 2008b, Mceligot *et al*. 2009, etc.). Gloss *et al*. (2010) concluded that an increased dissipation rate in the vicinity of the roughness elements is a physical mechanism that leads to an increased total head loss when walls are no longer smooth in laminar flows. However, the entropy theory applied in hydro-machine is relatively few. Gong *et al*. (2013) successfully applied entropy analysis for hydraulic losses in a Francis turbine. He concluded that the method of entropy production analysis had advantages of determining the energy dissipation and its exact location. Li *et al*. (2016) analyzed the hump characteristic of a pump turbine using the Entropy Production method and proved that the method can be used to predict the losses in the turbine from the view of the thermodynamics.

The paper will deeply investigate the energy dissipation occurs in a pump turbine and validate the reason of the energy losses based on the entropy production theory and give a further sight into the mechanism of S characteristic of pump turbine.

2. ENTROPY PRODUCTION THEORY

Energy dissipation is related to entropy production, and entropy production is resulted from an irreversible thermodynamic process. Due to the complicated fluid flow in turbo machinery, certain mechanical energy is converted into internal energy for two reasons, the viscous stress within the boundary layer and the turbulent fluctuation stress in high Reynolds-number regions, without considering the heat transfer. As a result, the dissipation of mechanical energy can be computed from the viewpoint of thermodynamic using the entropy production theory.

The specific entropy production rate $\dot{S}_D'''$ can be defined as Eq.(1) (Bejan 1994):

$$\dot{S}_D''' = \frac{\dot{Q}}{T} \tag{1}$$

Where $\dot{Q}$ represents the energy transfer rate.

For steady turbulent flows, $\dot{S}_D'''$ is made up of two parts: one caused by time-averaged movement, and the other is caused by velocity fluctuations named the turbulent dissipation terms.

So, $\dot{S}_D'''$ can be expressed as Eq.(2) (SCHMANDT *et al*. 2011):

$$\dot{S}_D''' = \dot{S}_{\overline{D}}''' + \dot{S}_{D'}''' \tag{2}$$

Where $\dot{S}_{\overline{D}}'''$ and $\dot{S}_{D'}'''$ represent the specific entropy production rate due to the time-averaged movement and the specific entropy production rate due to velocity fluctuations respectively, which can be calculated as follows (Bejan 1996):

$$\dot{S}_{\overline{D}}''' = \frac{2\mu_{\text{eff}}}{T}\left[\left(\frac{\partial \overline{u_1}}{\partial x_1}\right)^2 + \left(\frac{\partial \overline{u_2}}{\partial x_2}\right)^2 + \left(\frac{\partial \overline{u_3}}{\partial x_3}\right)^2\right] + \frac{\mu_{\text{eff}}}{T}\left[\left(\frac{\partial \overline{u_2}}{\partial x_1} + \frac{\partial \overline{u_1}}{\partial x_2}\right)^2 + \left(\frac{\partial \overline{u_3}}{\partial x_1} + \frac{\partial \overline{u_1}}{\partial x_3}\right)^2 + \left(\frac{\partial \overline{u_2}}{\partial x_3} + \frac{\partial \overline{u_3}}{\partial x_2}\right)^2\right] \tag{3}$$

$$\dot{S}_{D'}''' = \frac{2\mu_{eff}}{T}\left[\left(\frac{\partial u_1'}{\partial x_1}\right)^2 + \left(\frac{\partial u_2'}{\partial x_2}\right)^2 + \left(\frac{\partial u_3'}{\partial x_3}\right)^2\right] +$$

$$\frac{\mu_{eff}}{T}\left[(\frac{\partial u_2^{'}}{\partial x_1}+\frac{\partial u_1^{'}}{\partial x_2})^2+(\frac{\partial u_3^{'}}{\partial x_1}+\frac{\partial u_1^{'}}{\partial x_3})^2+(\frac{\partial u_2^{'}}{\partial x_3}+\frac{\partial u_3^{'}}{\partial x_2})^2\right] \tag{4}$$

Where $\overline{u_1}$, $\overline{u_2}$ and $\overline{u_3}$ represent time-averaged velocity components, and $u_1^{'}$, $u_2^{'}$ and $u_3^{'}$ indicate velocity fluctuation components; μ_{eff} is the effective viscosity, which can be expressed by Eq. (5):

$$\mu_{eff}=\mu+\mu_t \tag{5}$$

Where μ_t stands for the turbulent viscosity.

But, $\dot{S}_{D'}^{'''}$ is unavailable because the fluctuation velocity component is not obtainable when the results of simulations are obtained by the RANS numerical method. According to Mathieu *et al.* (2000) and Kock *et al.* (2004), the variable ε introduced in most turbulence models corresponds to $\dot{S}_{D'}^{'''}$ when *Re* converges towards ∞. $\dot{S}_{D'}^{'''}$ can be expressed as Eq.(6):

$$\dot{S}_{D'}^{'''}=\frac{\rho\varepsilon}{T}=\frac{\beta\rho\omega k}{T} \tag{6}$$

Where ε stands for the dissipation rate of kinetic energy. $\beta=0.09$. Here, ω represents the characteristic frequency and k is the kinetic energy of the turbulent fluctuations in the SST k-ω turbulence model. Then the whole entropy production rate can be obtainable follow by integration over the overall flow field volume V:

$$\dot{S}_{\overline{D}}=\int_V \dot{S}_{\overline{D}}^{'''}\mathrm{d}V \tag{7}$$

$$\dot{S}_{D'}=\int_V \dot{S}_{D'}^{'''}\mathrm{d}V \tag{8}$$

$$\dot{S}_D=\dot{S}_{\overline{D}}+\dot{S}_{D'}=\int_V \dot{S}_D^{'''}dV \tag{9}$$

Where $\dot{S}_D$, $\dot{S}_{\overline{D}}$ and $\dot{S}_{D'}$ stand for the whole entropy production rate for turbulent flows, the entropy production rate due to the time-averaged movement and the entropy production rate due to velocity fluctuations respectively.

Then, we can get $\dot{S}_D^{'''}$ at every point and $\dot{S}_D$ at the overall flow field via post processing of simulation results in the whole flow passage. We can obtain the energy dissipation distribution and specific positions where they occur clearly by entropy production analysis.

3. COMPUTATIONAL MODEL AND NUMERICAL METHODS

3.1 Computational Domain

The computational domain includes spiral casing, stay vanes, guide vanes, runner and draft tube as shown in Fig. 1. The numerical simulation is carried out when the different components are connected together by three interfaces. The parameters of the reduced model pump turbine are shown in Table 1.

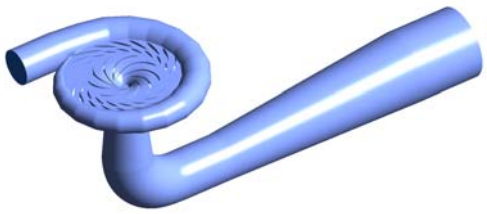

Fig. 1. Computational domain.

Table 1 Parameters of the model pump turbine

Parameter	Value
Runner inlet diameter D_1 (mm)	524
Number of runner blades Z_b	9
Number of stay vanes *Zs*	20
Number of guide vanes *Zg*	20
Height of guide vane *Hg* (mm)	45.77

3.2 Computational Grid

The mesh of scaled pump turbine was generated in structured grids with ANSYS ICEM. Local refinements for the boundary layers were done to get appropriate value of y^+, and the grids of different parts are shown in Fig. 2.

3.3 Numerical Methods

In this paper, the simulations were conducted by the commercial CFD code ANSYS CFX In order to capture flow details in boundary layers better and get more precise results, SST k-ω turbulence model was used. A mass flow inlet and a pressure outlet that came from experiments were given as the boundary conditions, and the walls were set to be no-slip and the standard wall function was used to simulate the near wall flow. All simulations were carried out without considering heat transfer and the occurrence of cavitation, and they were all in steady state.

3.4 Validation of Grid Independence

The verification of grid independence was performed with respect to the hydraulic head and efficiency of the model pump turbine which could be calculated by Eq.(10) and Eq.(11) respectively. Fig. 3 reflects how the hydraulic head and efficiency of the model pump turbine vary with the grid number. It indicates that the hydraulic head and efficiency of the model pump turbine increase a little when the grid number is higher than 5.46 million. The final grids with a nodes number of 9.96 million was employed.

$$H=\frac{P_{in}-P_{out}}{\rho g} \tag{10}$$

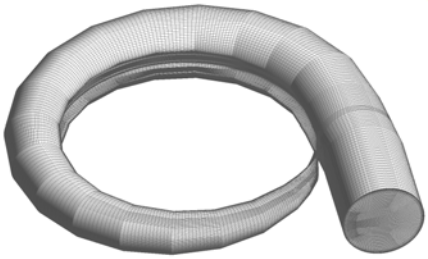

a) Spiral casing

b) Stay-guide vanes

c) Runner

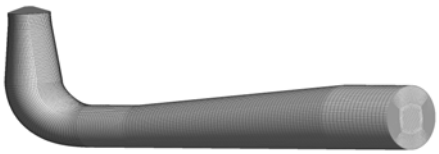

d) Draft tube

Fig. 2. Grids of different components.

$$\eta = \frac{T\Omega}{\rho g H Q} \tag{11}$$

Where P_{in} and P_{out} are the average pressure at spiral casing inlet and draft tube outlet respectively. ρ is the density of water and g is the acceleration due to gravity. T is the torque of runner. Ω is the rotational angler speed of runner. Q is the volume flow rate of the turbine.

Three different grid densities (fine-G1 with grid number of 9.96 million, medium-G2 with grid number of 6.62 million, and coarse-G3 with grid number of 4.43 million) were used to carry out the grid sensitivity check. The type G3-type mesh was the coarsest mesh in the simulation. The subsequent mesh was updated by 1.5X in the grid number. The grid quality was taken into consideration at each step of grid creation, so that the mesh nodes did not correspond exactly to a 1.5X increase. The simulations were performed at the 45.5% guide vane opening, and operating condition n_{11}=35.529 r·m$^{1/2}$·min^{-1}, Q_{11}=0.3194 m$^{1/2}$/s, for all grid types. The Grid Convergence Index (GCI) method was used to evaluate the numerical uncertainties and grid convergence. The extrapolation values and uncertainty in the grid convergence were estimated using the GCI method (Celik *et al*. 2008): the computed flow parameters are established in Table 2. And Fig. 3 shows the grid check results. The approximate and extrapolated relative errors were estimated as:

$$e_a^{21} = \left| \frac{G_1 - G_2}{G_1} \right| \tag{12}$$

$$e_{ext}^{21} = \left| \frac{G_{ext}^{21} - G_2}{G_{ext}^{21}} \right| \tag{13}$$

$$G_{ext}^{21} = (r_{21}^{} G_1 - G_2)/(r_{21}^{} - 1) \tag{14}$$

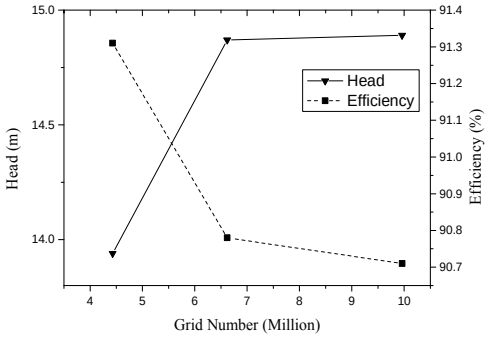

Fig. 3. Validation of grid for head and efficiency. Experimental head is 14.92 and experimental efficiency is 85.51 for the validated condition.

Table 2 Computed flow parameters. Experimental head is 14.92 and experimental efficiency is 85.51 for the validated condition

Parameter	Turbine head (H)	Turbine efficiency (η)
r_{21}	1.5	1.5
r_{32}	1.5	1.5
G_1	14.89	90.71
G_2	14.87	90.78
G_3	13.94	91.31
G_{ext}^{21}	14.890439	90.69935
e_a^{21}	0.0013432	0.000772
e_{ext}^{21}	0.0000295	0.000117
GCI_{fine}^{21}	0.0000369	0.000147
GCI_{med}^{32}	0.0017182	0.001111

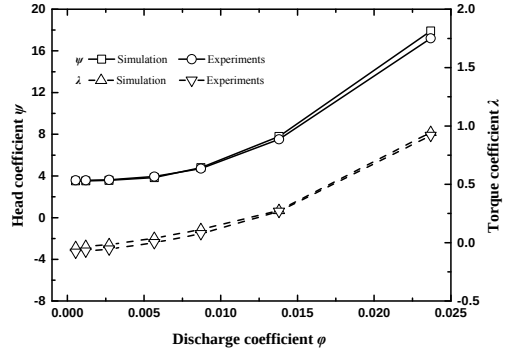

a) External characteristic curve at5mm

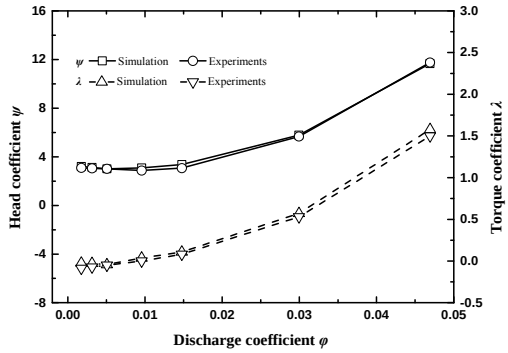

b) External characteristic curve at 10mm

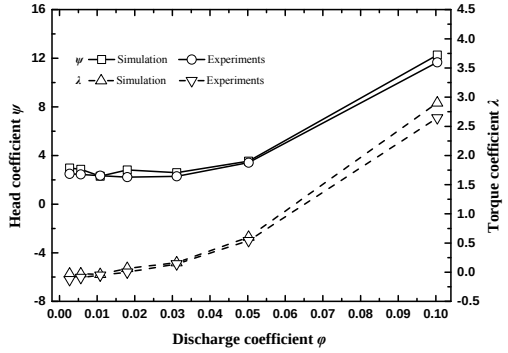

c) External characteristic curve at 32mm

Fig. 7. External characteristic curve at different guide vane openings.

The GCI from G2 to G1 was very low compared to the GCI from G3 to G2. And the turbine head and efficiency with the fine grid is closer to the experimental results. The converged solution with the fine grid (G1 with grid number of 9.96 million) was used for further simulations at different operating conditions.

4. ENTROPY PRODUCTION ANALYSIS FOR S-SHAPE CHARACTERISTICS

4.1 Experiment validation

4.1.2 Comparison of Complete Characteristics

All numerical simulations carried out in the paper were based on the conditions at the guide vane opening of 5mm, 10mm and 32mm. The comparisons of hill curves of the hydro turbine with experimental results were shown in Fig. 4-Fig. 6.

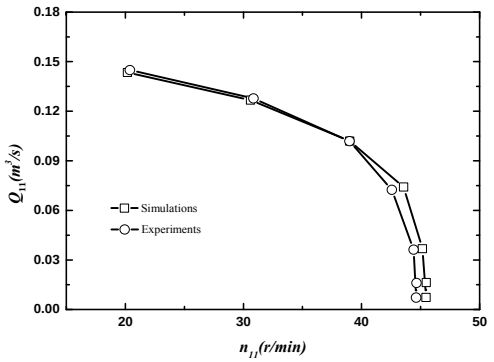

Fig. 4. Characteristic curve at 5mm.

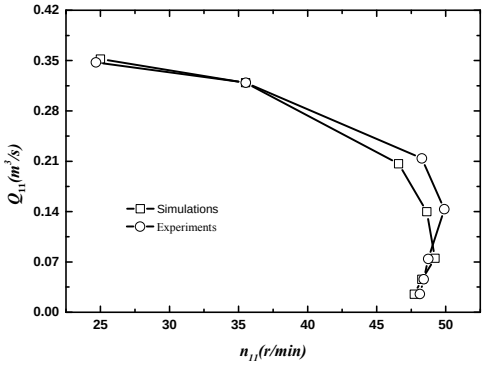

Fig. 5. Characteristic curve at 10mm.

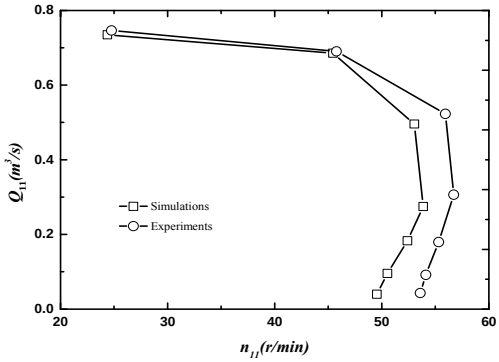

Fig. 6. Characteristic curve at 32mm.

It can be implied from these figures that the simulations coincide with experiments well when the turbine works at turbine mode under the three different guide vane openings, and the coincidences become worse when the pump turbine goes into runaway speed operating conditions neighborhood and braking conditions, which may be due to the fact that the flow becomes more complex in these conditions. The "S" characteristics are more obvious with the bigger guide vane opening. The simulation results have a quite good agreement with experimental results under the guide vane opening of 5mm, and the agreements become a little worse when the guide vane opening increases.

4.1.2 Comparison of External Characteristics

To compare external characteristics of the turbine between experiments and simulations, we defined several parameters, which are discharge coefficient φ, head coefficient ψ and torque coefficient λ:

$$\psi = \frac{2gH}{R_1^2\Omega^2} \tag{15}$$

$$\varphi = \frac{Q}{\pi R_1^2\Omega} \tag{16}$$

$$\lambda = \frac{T}{\pi R_1^5\Omega^2} \tag{17}$$

Where, g represents the acceleration due to gravity (ms^{-2}); H represents the hydraulic head (m); R_1represents the runner inlet radius (m); Ω represents the rotational speed of runner ($rad{\cdot}s^{-1}$); Q represents the discharge ($m^3{\cdot}s^{-1}$); T represents the sum total of the individual torque of the runner blades (N·m); ρ represents the density of fluid ($kg{\cdot}m^{-3}$).

Figure 7 shows the comparisons of three coefficients with experiment results. The head coefficient error is less than 3% in most operating conditions even if the error is nearly 4% in large discharge operation conditions when it is at 5mm guide vane opening. The head coefficient error is less than 4% in most operating conditions, but the error is nearly 9% when discharge coefficient φ=0.0148.The head coefficient error becomes even much bigger at 32mm guide vane opening. So a conclusion can be drawn that the head coefficient error is larger when guide vane opening is bigger. From the comparison results of torque coefficient, we can see that the torque coefficient is consistent with experimental results well and the condition point of biggest error happens at the largest discharge. The torque coefficient error is also larger when guide vane opening is bigger.

To sum up, the simulation results are consistent with experimental results well, so further analyses can be done based on the numerical simulations.

4.2 Variation of Overall Entropy Production

Figure 8 shows the changes of overall entropy production at three different guide vane openings. Entropy production indicates that waves and instability become strengthened with the increase of the discharge, which may be due to the transform between braking mode and turbine mode. But entropy production is not big in the braking modes although the flow is complicated. The reasons probably are that the speed is quite small when discharge is not big and the losses coming from flow attacking are also small. There exists minimum values under 5mm (φ=0.0087), 10mm (φ=0.0299), 32mm (φ=0.0503) guide vane openings which are all in turbine mode, which indicates entropy production reaches the smallest value in the relatively small discharge when the pump turbine goes into stable turbine mode. The values of entropy production grow fast when the pump turbine goes into stable turbine mode, and the maximum values all happen under the biggest discharge and they are all almost the same size at different guide vane openings.

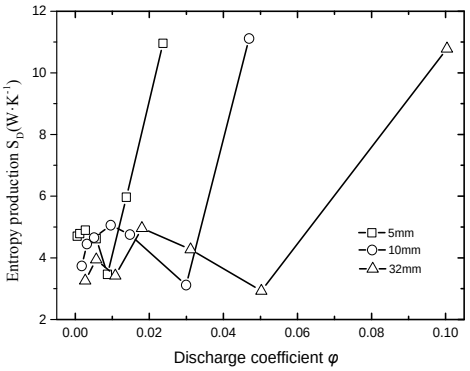

Fig. 8. Overall entropy production at different guide vane openings.

Figure 9 shows the detailed information of entropy production for different components at different guide vane openings. It can be concluded that the entropy production of spiral casing accounts for the minimum proportion in all components and it is not more than 1% in almost all operating conditions, which indicates that the design of spiral casing obtains good effect to reduce losses. In addition, the entropy production of spiral casing is bigger with the increase of discharge. The entropy production of blade cascades and runner has relatively large fluctuations at different guide vane openings, and it features "S" characteristics with the change of discharge, which illustrates that the flow is complicated in the components and changes sharply with the increase of discharge. The entropy production of runner accounts for the largest proportion when discharge is small. However the components whose entropy production accounts for the largest proportion vary with the increase of guide vane openings when discharge reaches the biggest value, and they are blade cascades (5mm), runner (10mm) and draft tube (32mm) respectively.

4.3 Analysis of Entropy Production Distribution

Because the S characteristics is the most obvious and the simulation results are consistent with experimental results well in the 10mm guide vane opening, further study was applied at the 10mm guide vane opening. In order to analyze the internal flow losses during the "S" region better, five operating points A (n_{11}= 46.59, Q_{11}=0.2065), B(n_{11}=48.63, Q_{11}= 0.1397), C(n_{11}= 49.22, Q_{11}=0.0750), D(n_{11}= 48.28, Q_{11}= 0.0457), E(n_{11}=47.72, Q_{11}= 0.0251) shown in Fig.10 are chosen for analysis based on the entropy production theory. Since the losses of the pump turbine in "S" region mainly happen in the runner, blade cascades, and draft tube, the following analysis are on these components.

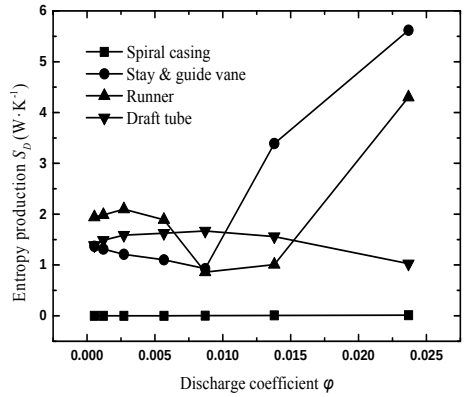

a) Entropy production of different components at 5mm

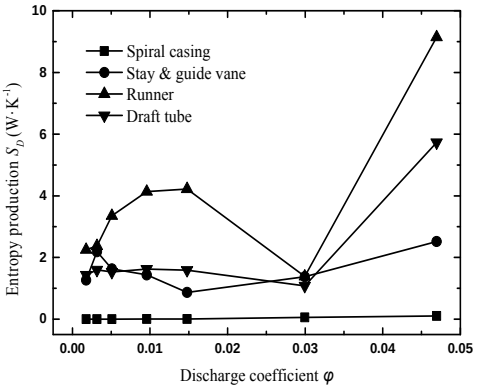

b) Entropy production of different components at 10mm

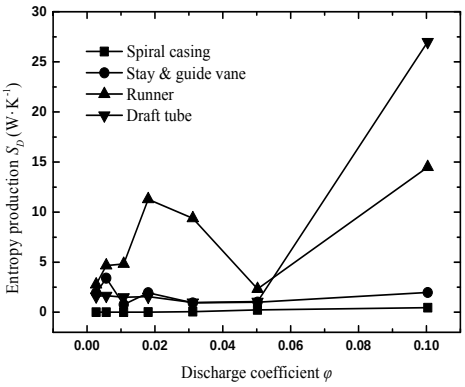

c) Entropy production of different components at 32mm

Fig. 9. Entropy production of different components at different guide vane openings.

4.3.1 Analysis of the Distributor

As parts of the distributor core components, stay vanes and guide vanes play a very important role in receiving the flow from the spiral casing and guiding it into the runner. In order to analyze guide vanes and stay vanes for more details, the height of the vanes was set 0 to 1 from the band to the crown. Span 0.1 is the plane near the band, Span 0.9 is the plane near the crown, and Span 0.5 is the plane in the middle of the two as shown in Fig. 11. The three planes were chosen to make further analysis.

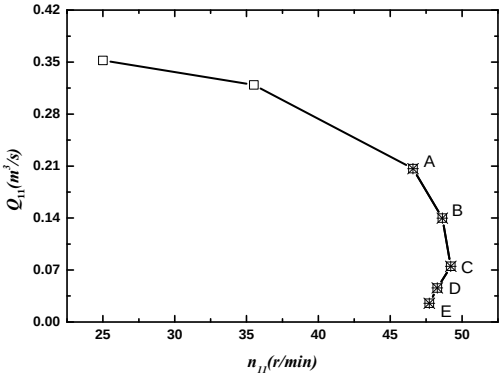

Fig. 10. Operating points for analysis.

Fig. 11. Spanwise plane of the blade cascades.

The entropy production rate (EPR) distribution of guide vanes and stay vanes in three spans is shown in Fig.12 to Fig.14. It can be seen that the EPR of guide vanes is much higher than that of stay vanes, which reveals that the energy loss in the guide vane space is much more than that in stay vane space and the design of stay vanes is very suitable to reduce the energy losses. The high value of EPR is mainly located on tail area of stay vanes and the vaneless space. The flow is very complex in vaneless space, and large energy losses may be caused by flow separation happening at the tail of stay vanes and the impact of flow on runner blades, and the effect of runner rotation strengthens the flow disorder. The operating point D which has the biggest rotational speed (500.437rpm) has the largest EPR in the interface area of distributors and runner, which, again, illustrates that runner rotary motion will affect the energy loss in the turbine especially the vaneless space. In general, the distribution of EPR is axially symmetric along the circumferential direction. Additionally, the results also reveal that the EPR increases gradually from the band to the crown along the blade height direction.

4.3.2 Analysis of the Runner

Since the entropy production of runner accounts the largest proportion in all operating points at 10mm guide vane opening, it is very important to analyze the flow losses of runner more carefully. Similar to the above, three planes were obtained by expanding blade to blade surface along the spanwise direction, chosen planes are shown in Fig. 15.

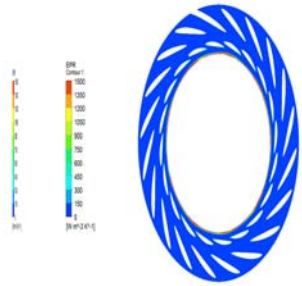

a) Operating condition A

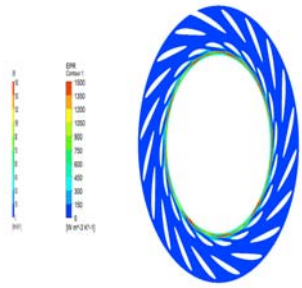

b) Operating condition B

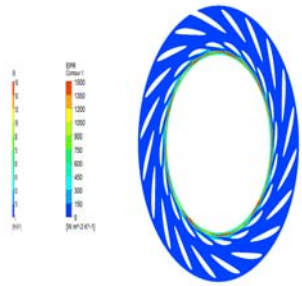

c) Operating condition C

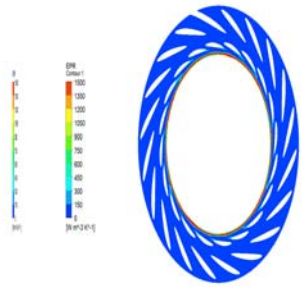

d) Operating condition D

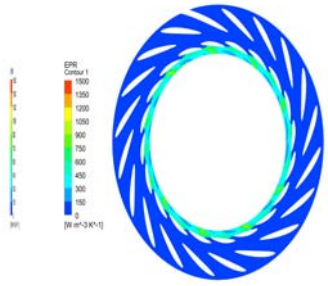

e) Operating condition E

Fig. 12. EPR distribution of Span 0.1 in the blade cascades.

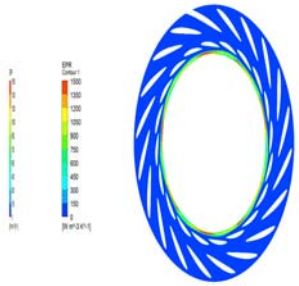

a) Operating condition A

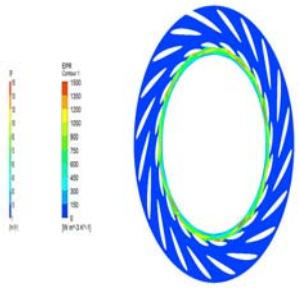

b) Operating condition B

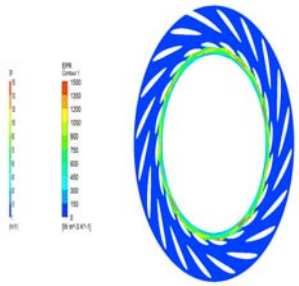

c) Operating condition C

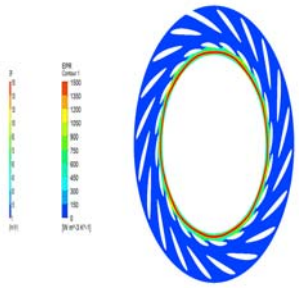

d) Operating condition D

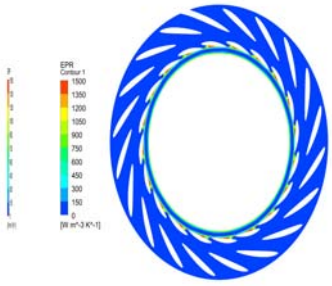

e) Operating condition E

Fig. 13. EPR distribution of Span 0.5 in the blade cascades.

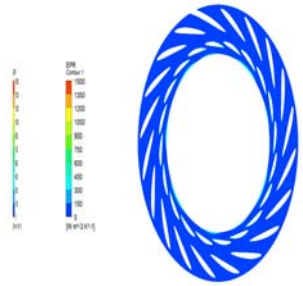

a) Operating condition A

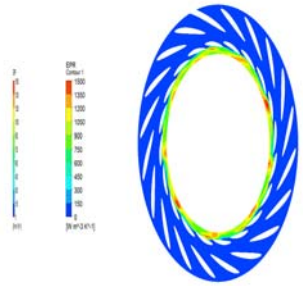

b) Operating condition B

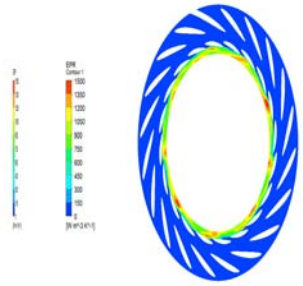

c) Operating condition C

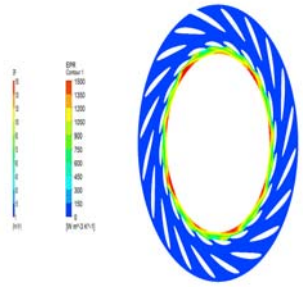

d) Operating condition D

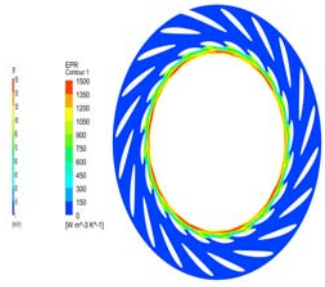

e) Operating condition E

Fig. 14. EPR distribution of Span 0.9 in the blade cascades.

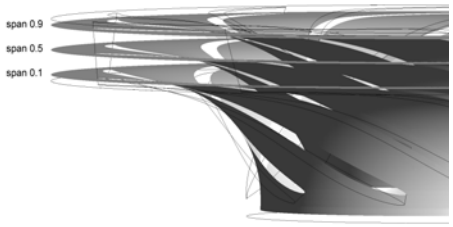

Fig. 15. Spanwise planes of the runner.

The simulation results were shown in Fig. 16 to Fig. 18. It can be seen that EPR distribution of runner shows a similar profile and high EPR mainly happens in the leading edges of the blades near passage inlet, which may be caused by the violent impact of flow. EPR is also very high in the trailing edges near runner passage outlet. But EPR has relatively smaller value on the medium flow surface and the outlet area of runner near the crown.

The distribution of EPR also indicates that there exists backflow in the entrance edges of blades and flow separation in the exit edges near the band. Fig.16 to Fig.18 show that EPR in the runner passage outlet becomes higher gradually with the reduction of discharge from A to E, but EPR in the runner passage inlet becomes higher from A to B corresponding to turbine conditions and becomes smaller from C to E corresponding to braking conditions. Above results indicates that the blade wake near passage outlet is enhanced with the reduction of discharge and the energy losses are bigger, but the impact of flow in the leading edges of the blades near passage inlet intensifies with the reduction of discharge in turbine conditions and begins to weaken in braking conditions. It can be also seen that the location of the highest EPR in the blades surfaces changes from the crown to the band. Generally speaking, EPR is higher on the pressure surface of blades than that on the suction surface in the inlet near the band, however the value is higher on the suction surface of blades than that on the pressure surface in the inlet near the crown. The highest EPR mainly focuses on the tip of blades in the outlet near the band, which indicates the wake effect results in serious energy losses. However the highest value mainly focuses on the suction surface in the outlet near the crown. Moreover, the EPR of span 0.1 and span 0.9 is higher than that of span 0.5, and the phenomenon may result from the effect of the boundary layer near the band and the crown, in which viscosity action causes the losses of energy.

4.3.3 Analysis of the Draft tube

Figure 19 presents the EPR distribution results of cross section in the draft tube. It can be seen that the largest energy losses mainly lie at the wall of straight cone near the inlet of draft tube, which may be due to the intense vortex flow. Secondly the energy losses at the inner surface of elbow are also very high, which may be caused by secondary flow resulting from the turning of the flow. The area of central part in the inlet of draft tube and the area near the outside surface of elbow have relatively high EPR. Moreover, the EPR in the area of central part in the inlet of draft tube is higher with the reduction of discharge from A to E, the reason may be that the stagnation region of central area expands with the reduction of flow velocity in the inlet of draft tube.

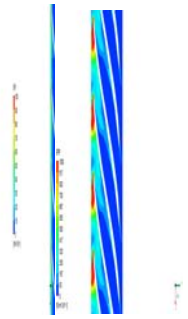

a) Operating condition A

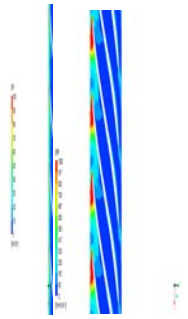

b) Operating condition B

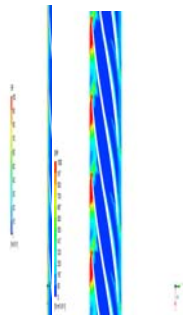

c) Operating condition C

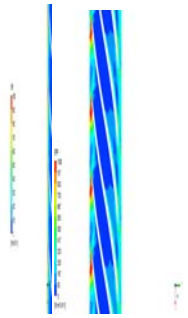

d) Operating condition D

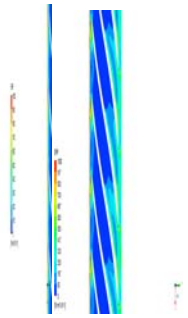

e) Operating condition E

Fig. 16. EPR distribution of Span 0.1 in the runner passage.

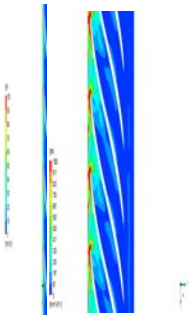

a) Operating condition A

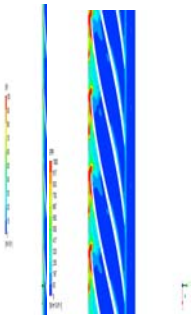

b) Operating condition B

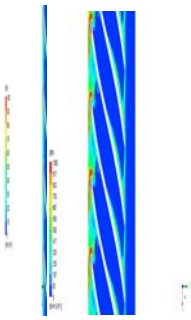

c) Operating condition C

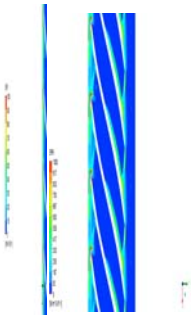

d) Operating condition D

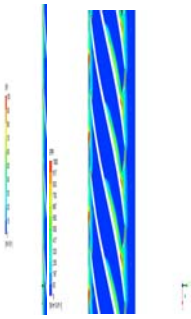

e) Operating condition E

Fig. 17. EPR distribution of Span 0.5 in the runner passage.

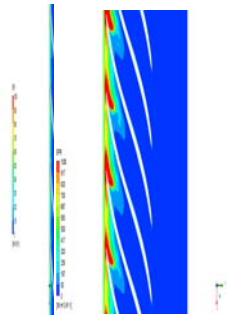

a) Operating condition A

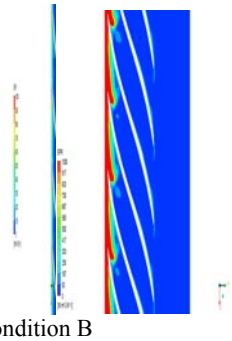

b) Operating condition B

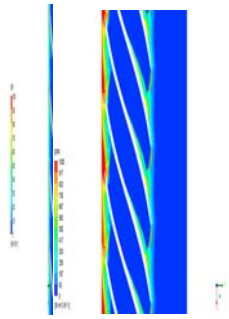

c) Operating condition C

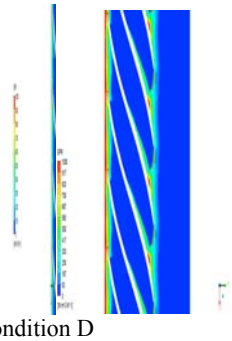

d) Operating condition D

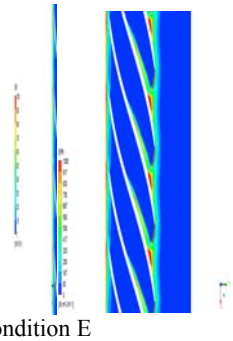

e) Operating condition E

Fig. 18. EPR distribution of Span 0.9 in the runner passage.

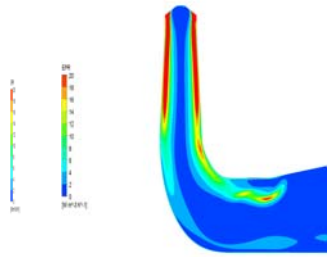

a) Operating condition A

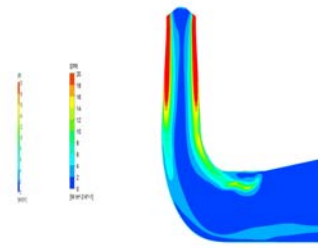

b) Operating condition B

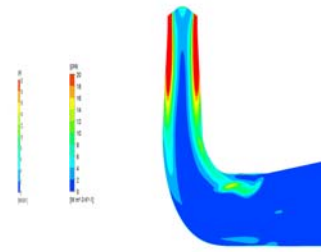

c) Operating condition C

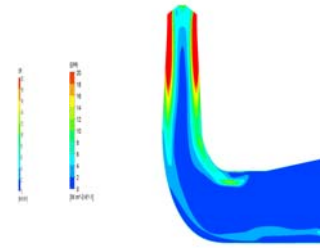

d) Operating condition D

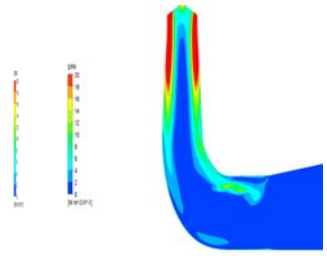

e) Operating condition E

Fig. 19 EPR distribution of cross section in the draft tube.

5. CONCLUSION

Steady simulations of full passages were applied for the pump turbine at 5mm, 10mm and 32mm guide vane openings respectively in this paper, and the analyses were made based on the entropy production

theory. Some conclusions can be drawn as follows.

(1) It is effective to estimate the energy dissipation of pump turbine with the entropy production theory, and the losses in the turbine can be correctly located.

(2) The entropy production is not big in the braking modes of "S" region although the flow is complicated. The reasons probably are that the speed is quite small when discharge is not big and the losses coming from flow attacking are also small. The entropy production reaches the smallest value in the relatively small discharge when the pump turbine goes into stable turbine mode.

(3) The entropy production of spiral casing accounts for the minimum proportion in all components. The entropy production of blade cascades and runner has relatively large fluctuations at different guide vane openings, and it features S-shape characteristics with the increase of discharge, which illustrates that the flow is complicated in the components.

(4) The EPR of guide vanes is much higher than that of stay vanes, and the high value of EPR is mainly focus on tail area of stay vanes and the interface area of distributors and runner. The highest EPR mainly happens in the leading edges of the blades near passage inlet in the runner. The above energy losses are mainly caused by flow separation and flow impact. In addition, the high energy losses mainly lie at the wall of straight cone near the inlet and the inner surface of elbow in draft tube, which are caused by the vortex flow and the secondary flow.

ACKNOWLEDGEMENTS

The authors would like to thank *the Fundamental Research Funds for the Central Universities* (Grant No. HIT. NSRIF2017046) for the support.

REFERENCES

Bejan, A. (1994). *Entropy Production through Heat and Fluid Flow*. John Wiley and Sons, Chichester, UK..

Bejan, A. (1996). *Entropy production minimization: the method of thermodynamic optimization of finite-time systems and finite-time processes*. CRC Press, Boca Raton.

Celik, I. B., U. Ghia, P. J. Roache, C. J Freitas, H. Coleman and P. E. Raad (2008). Procedure for Estimation and Reporting of Uncertainty due to Discretization in CFD *Applications. ASME Journal of Fluids Engineering* 130, 078001.

Ghasemi, E., D. M. Mceligot, K. P. Nolan, J. Crepeau, A. Tokuhiro and R. S. Budwig (2013). Entropy generation in a transitional boundary layer region under the influence of free stream turbulence using transitional RANS models and DNS. *International Communication in Heat and Mass Transfer* 41, 10-16.

Gloss, D., and H. Herwig (2010). Wall roughness effects in laminar flows: an often ignored though significant issue. *Experiment in Fluids* 49, 461-470.

Gong, R. Z., H. J. Wang, L. X. Chen, D. Y. Li, H. C. Zhang and X. Z. Wei (2013). Application of entropy production theory to hydro-turbine hydraulic analysis. *Science China-Technological Sciences* 56(7), 1636-16437

Herwig, H., D. Gloss and W. Wenterodt (2008). A new approach to understanding the influence of wall roughness on friction. *Journal of Fluid Mechanical* 613, 35-53.

Kock, F. and H. Herwig (2004). Local entropy production in turbulent shear flows: a high Reynolds number model with wall functions. *International Journal of Heat and Mass Transfer* 47, 2205-2215.

Li, D. Y., R. Z. Gong, H. J. Wang, G. M. Xiang, X. Z. Wei and D. Q. Qin (2016). Entropy Production Analysis for Hump Characteristics of a Pump Turbine Model. *Chinese Journal of Mechanical Engineering* 27(4), 803-812.

Mathieu, J. and J. Scott (2000). *An introduction to turbulent flow*. Cambridge University Press, UK..

Mceligot, D. M., E. J. Walsh, E. Laurien and P. R. Spalart (2008a). Entropy generation in the viscous part of turbulent boundary layers. *ASME Journal of Fluids Engineering 130*(6), 061205.

Mceligot, D. M., K. P. Nolan, E. J. Walsh and E. Laurien (2008b). Effects of pressure gradients on entropy production in the viscous layers of turbulent wall flows. *International Journal of Heat and Mass Transfer 51*(5-6), 1104-1114.

Mceligot, D. M., R. S. Brodkey and H. Eckelmann (2009). Laterally converging duct flows: part 4. Temporal behavior in the viscous layer. *Journal of Fluid Mechanics* 634,433–461.

Naterer, G. F. and J. A. Camberos (2008). *Entropy-based design and analysis of fluids engineering systems*. CRC Press, Boca Raton.

Schmandt, B., and H. Herwig (2011). Internal flow losses: a fresh look at old concepts. *ASME Journal of Fluids Engineering* 133, 051201.

Zhang, H. C., B. Schmandt and H. Herwig (2009). Determination of loss coefficients for micro-flow devices: a method based on the second law analysis (SLA). *ASME 2009 2nd Micro/Nanoscale Heat & Mass Transfer International Conference*, Shanghai, China.